Biogeosciences Discuss., 12, 15011–15050, 2015
www.biogeosciences-discuss.net/12/15011/2015/
doi:10.5194/bgd-12-15011-2015

Biogeosciences Discussions
Open Access

Climate, CO_2, and demographic impacts on global wildfire emissions

W. Knorr[1], L. Jiang[2], and A. Arneth[3]

[1]Physical Geography and Ecosystem Analysis, Lund University, Sölvegatan 12, 22362 Lund, Sweden
[2]National Center for Atmospheric Research, Boulder, Colorado, USA
[3]Division of Ecosystem-Atmosphere Interactions, KIT/IMK-IFU, Garmisch-Partenkirchen, Germany

Received: 29 July 2015 – Accepted: 25 August 2015 – Published: 11 September 2015

Correspondence to: W. Knorr (wolfgang.knorr@nateko.lu.se)

Published by Copernicus Publications on behalf of the European Geosciences Union.

Abstract

Wildfires are by far the largest contributor to global biomass burning and constitute a large global source of atmospheric traces gases and aerosols. Such emissions have a considerable impact on air quality and constitute a major health hazard. Biomass burning also influences the radiative balance of the atmosphere and is thus not only of societal, but also of significant scientific interest. There is a common perception that climate change will lead to an increase in emissions as hot and dry weather events that promote wildfire will become more common. However, even though a few studies have found that the inclusion of CO_2 fertilization of photosynthesis and changes in human population patterns will tend to somewhat lower predictions of future wildfire emissions, no such study has included full ensemble ranges of both climate predictions and population projections, including the effect of different degrees of urbanisation.

Here, we present a series of 124 simulations with the LPJ-GUESS-SIMFIRE global dynamic vegetation – wildfire model, including a semi-empirical formulation for the prediction of burned area based on fire weather, fuel continuity and human population density. The simulations comprise Climate Model Intercomparison Project 5 (CMIP5) climate predictions from eight Earth system models using two Representative Concentration Pathways (RCPs) and five scenarios of future human population density based on the series of Shared Socioeconomic Pathways (SSPs), sensitivity tests for the effect of climate and CO_2, as well as a sensitivity analysis using two alternative parameterisations of the semi-empirical burned-area model. Contrary to previous work, we find no clear future trend of global wildfire emissions for the moderate emissions and climate change scenario based on the RCP 4.5. Only historical population change introduces a decline by around 15 % since 1900. Future emissions could either increase for low population growth and fast urbanisation, or continue to decline for high population growth and slow urbanisation. Only for high future climate change (RCP8.5), wildfire emissions start to rise again after ca. 2020 but are unlikely to reach the levels of 1900 by the end of the 21st century. We find that climate warming will generally increase the risk of

fire, but that this is only one of several equally important factors driving future levels of wildfire emissions, which include population change, CO_2 fertilisation causing woody thickening, increased productivity and fuel load, and faster litter turnover in a warmer climate.

1 Introduction

Wildfires are responsible for approximately 70 % of the global biomass burned annually (van der Werf et al., 2010, updated). Emissions from wildfires in the form of trace gases and aerosols can have a considerable impact on the radiative balance of the atmosphere (Langmann et al., 2009) and also constitute a large source of atmospheric pollutants (Kasischke and Penner, 2004). At the same time, wildland fires are an important component of terrestrial ecosystems (Bowman et al., 2009) and the Earth system in (Arneth et al., 2010). Fires respond to changes in climate, vegetation composition and human activities (Krawchuk et al., 2009; Pechony and Shindell 2010; Kloster et al., 2012; Moritz et al., 2012), with some model simulations showing a positive impact of climate change on emissions during the 21st century, but a negative, albeit smaller, impact due to changes in land use and increased fire suppression (Kloster et al., 2012).

Empirical studies designed at isolating the effect of human population density – here used as an aggregate value representing human interference at the landscape scale – have generally shown that higher population density per se leads to a decrease in the annual area burned (Archibald et al., 2008; Knorr et al., 2014; Bistinas et al., 2014), even though there is a common perception that wildfire activity peaks at intermediate levels of population density. This apparent paradox was shown to be the result of co-variations between population density and other factors such as fuel load or flammability – if these co-variations are taken into account, the view of a negative impact is consistent with the observed peak (Bistinas et al., 2014).

The main future drivers of changing wildfire have potentially opposing effects on emissions – temperature (increasing), CO_2 via productivity (increasing), CO_2 via woody

thickening (Buitenwerf et al., 2012; decreasing), and human population density (decreasing emissions). In the meantime, socio-demographic change, interacting with other economic and technological factors, may also lead to climate change – e.g. slow population growth combined with a conventional development pathway of high fossil fuel dependence would result in high CO_2 emissions and large temperature increases. Moreover, the same population growth but with different urbanization trends could also lead to different levels of spatial population distributions and concentrations, and consequently different results concerning wildfire emissions. Therefore, it is important to first assess the impact of each factor individually before arriving at conclusions concerning aggregate effects. Another important point of consideration is that if climate forcing is based on a model with low climate sensitivity to CO_2 change (i.e. relatively small change in global mean temperature simulated for a given rise in atmospheric CO_2), CO_2 effects might dominate over climate effects. The reverse applies to climate models with a high climate sensitivity. We therefore use an ensemble of climate models instead of only one or two, consider a wide range of future scenarios of population density change, and differentiate between the effects of changes in not only population sizes within a country, but also population spatial distribution via urbanisation.

While previous studies have focused on the task of predicting future wildfire emissions and have at most considered impacts of population changes separately to those of climate and CO_2, here we partition the projected changes into the following drivers: climate via changes in burned area, climate via changes in fuel load, CO_2 via changes in burned area, CO_2 via changes in fuel load, and population density considering both the effects of population growth and urbanisation. The goal is a better understanding of the underlying processes of wildfire emission changes, which should help establishing the necessary links between climate policy (emissions), climate science (climate sensitivity), demography, air pollution and atmospheric chemistry, as well as wildfire management.

2 Methods

2.1 Models and driving data

We use the coupled fire-vegetation model LPJ-GUESS-SIMFIRE (Knorr et al., 2014, 2015) to simulate establishment, growth and mortality of natural vegetation, fuel load, burned area and wildfire emissions under changing climate, CO_2 and human population density. LPJ-GUESS (Smith et al., 2001) is a global dynamic vegetation model that simulates potential vegetation as a mixture of user-defined plant functional types (PFTs) which compete with each other in so-called patches. Each PFT is characterized by a set of traits, such as leaf longevity and phenology, growth form and bioclimatic limits to establishment and survival. In these simulations, we use five patches per grid cell, and within each patch, LPJ-GUESS simulates several age cohorts. In "cohort mode", which is used here, all individuals of a cohort are assumed to have identical characteristics. We use PFTs designed for global simulations as given by Ahlström et al. (2012).

Fire impacts on vegetation are simulated at monthly intervals as described by Knorr et al. (2012). SIMFIRE predicts annual fractional burned area, A (the fraction of each grid cell burned per year, also denoted fire frequency) using the following equation:

$$A(y) = a(B)F^{b}N_{\max}(y)^{c}\exp(-ep) \quad (1)$$

Here, y is the fire year defined as in Knorr et al. (2012) in such a way that it never "cuts" the fire season into two, B is the biome type, F is annual potential fraction of absorbed photosynthetically active radiation (FAPAR), an approximation of vegetation fractional cover easily observed from satellites and here used as a measure of fuel continuity (Knorr et al., 2014), $N_{\max}$ is the annual maximum Nesterov Index based on daily diurnal temperature mean, T_{m}, range, T_{r}, and precipitation, P, and p is human population density. The Nesterov index used is given by Thonicke et al. (2010) as the cumulative sum of $T_{\mathrm{m}} \times (T_{\mathrm{r}} + 4\,\mathrm{K})$ over all consecutive days with more than 3 mm rainfall. $a(B)$, b, c, and e are global parameters derived by optimisation of SIMFIRE burned area against observed burned area from GFED3 (Giglio et al., 2010) on a spatial grid

and for the entire globe (Table 2, "GFED3", "All population densities" of Knorr et al., 2014). To derive monthly burned area, we use the average diurnal cycle of burned area derived from GFED3 for 2001–2010 using a variable spatial averaging radius around each grid cell which is at least 250 km but has a total burned area over the period of 10 000 km^2. Information on biome type is passed from LPJ-GUESS to SIMFIRE, where biome type is a discrete number ranging from one to eight, using FAPAR of woody and herbaceous vegetation and of vegetation of at least 2 m as well as geographic latitude as information. F in Eq. (1) is a bias corrected value derived from LPJ-GUESS simulated FAPAR, F_{s}, via:

$$F = 0.42\,F_{\mathrm{s}} - 0.15\,F_{\mathrm{s}}^{2} \quad (2)$$

LPJ-GUESS-SIMFIRE, in the following denoted "LPJ-GUESS", is driven by output from Earth system model (ESM) simulations from the CMIP5 project (Taylor et al., 2012) in a way mostly following Ahlström et al. (2012), where climate output of monthly mean temperature, precipitation and downward shortwave radiation is bias corrected using the mean observed climate for the period 1961–1990, and atmospheric CO_2 levels used by LPJ-GUESS are taken from the RCP scenarios as prescribed for CMIP5 (Meinshausen et al., 2011). In variance to the cited work, we use CRU TS3.10 (Harris et al., 2014) as climate observations, and we predict monthly mean diurnal temperature range and number of wet days per month based on linear regressions against mean temperature and precipitation, respectively. Simulations are carried out on an equal-area pseudo-1° grid, which has a grid spacing of $1^{\circ} \times 1^{\circ}$ at the equator and a wider E-W spacing towards the poles in order to conserve the average grid cell area per latitude band.

We use global historical gridded values of human population density from HYDE (Klein-Goldewijk et al., 2010) for simulations up to 2005. For future scenarios, no gridded data are available, but we use instead per-country values of total population and percentage of urban population. In order to generate gridded population density after 2005, we use separate urban and rural population density from HYDE for the year 2005

and re-scale both by the relative growth of each in each country. After this procedure, we multiply the population density of all grid cells representing each country by a constant factor such that the growth of the total population of the given country relative to the 2005 HYDE data matches that of the per-country total population scenario used.

2.2 Scenarios

We run simulations for two climate change scenarios from the Representative Concentration Pathways (RCP). Of these, RCP4.5 represents an approximate radiative forcing scenario typical of the majority of stabilization scenarios included in the Fourth Assessment of Report of the International Panel on Climate Change. The other, RCP8.5, is a typical case of high emissions resulting from a lack of enforced stabilization of greenhouse gases, leading to high levels of climate change (van Vuuren et al., 2011). In this study, we will consider both scenarios separately as two alternative futures without any assignment of relative probabilities.

Climatic trends simulated for the 20th century as well as for RCP4.5 and RCP8.5 are shown in Table 1 for different regions, for the eight-ESM ensemble mean and range. (For definition of regions see Sect. 2.4 and Fig. 4.) There is a spatially rather uniform warming trend of around half a °C during the 20th century roughly in accordance with observations (Harris et al., 2014), with inter-model differences larger than differences between regions. Precipitation declines slightly during the same period, most strongly for already dry Middle East, with generally rather large inter-model differences, in particular for Africa, Oceania and South Asia. Temperature change under the RCP4.5 scenario towards the end of the 21st century is around +2.5 °C for most regions, except for higher values for the two regions comprising most of the Arctic (North America, North Asia), while precipitation overall increases, albeit with considerable declines for Oceania and Middle East on average, and for South America and Africa for the their respective ensemble minima. For RCP8.5, global mean temperature change reaches as high as +5 °C, with North America, North Asia and Middle East exceeding this value. Precipitation changes are similar to RCP4.5, but with both the inter-model ranges and

the inter-region differences considerably amplified. (For example, there is an almost 40 % decline for Oceania for the ensemble minimum.)

For population scenarios, we use marker scenarios of the Shared Socioeconomic Pathways (SSPs; O'Neill et al., 2012; Jiang 2014). Following Knorr et al. (2015), we consider a total of five scenarios: SSP2 scenario with medium population growth and central urbanisation, two extreme scenarios with either high population growth and slow urbanisation (SSP3) or low population growth with fast urbanisation (SSP5), and two further scenarios in which the medium population growth (SSP2) is combined with either slow (SSP3) or fast (SSP5) urbanisation. Fur the purpose of analysis, we will consider these five scenarios equally plausible, keeping in mind, however, that this is mainly a working hypothesis.

2.3 Simulations

We combine output from eight EMSs with two different emissions pathways, one based on RCP4.5 and one on RCP8.5, all run with the medium population and central urbanisation scenario of SSP2. These 16 simulations are repeated six times using the other four population and urbanisation scenarios, one simulation each where population is held constant at 2000 levels, and one simulation where both population and atmospheric CO_2 levels are held constant at 2000 levels, giving $8 \times 2 \times 7 = 112$ simulations. To these we add two more sets of six simulations each with a different parameterisation of SIMFIRE, comprising runs using the SSP2 demographic scenario, fixed population, and fixed population and CO_2 and output from MPI-ESM-LR based on either RCP4.5 or RCP8.5. The first alternative SIMFIRE parameterisation is derived from a global optimisation against MCD45 burned area (Roy et al., 2008) according to Knorr et al. (2014, Table 2, "MCD45", "All population densities"), and the other assumes a slight increase in burned area with increasing population density if p is less than 0.1 inhabitants per km^2, where Eq. (1) is replaced by:

$$A(y) = (0.81 + 1.9p)a(B)F^b N_{\max}(y)^c \exp(-ep), \quad (3)$$

based on results presented by Knorr et al. (2014).

2.4 Analytical framework

Since the present analysis only considers wildfires, we exclude all grid cells that contain more than 50 % of cropland at any time during 1901–2100 in either the RCP6.0 or 8.5 land use scenarios (Hurtt et al., 2011). The threshold of 50 % is the same as used during SIMFIRE optimisation. A time-invariant crop mask is used in order to avoid introducing time trends in the results through temporal variations of the crop mask.

The changes in emissions may be caused by climate change alone, by changes in atmospheric CO_2, or by changes in population density. Emissions are determined by the product of burned area, the amount of fuel present, and the fraction of fuel combusted in a fire. Climate effects burned area directly by changing fire risk via N_{max}, while climate and CO_2 effect burned area indirectly by changing the vegetation type, which affects $a(B)$, or vegetation cover, which affects F in Eq. (1). Fuel load is also affected by vegetation productivity which is driven by both climate and CO_2, and by litter decay rates, which depend on temperature and precipitation (Smith et al., 2001). The combusted fraction of fuel mainly depends on the presence of grasses vs. trees (Knorr et al., 2012). Finally, population density affects emissions through burned area via Eq. (1).

In order to assess the effect of different driving factors on changing emissions, we employ the following analytical framework:

$$E_{T2} = E_{T1} + \Delta E_{\text{clim}} + \Delta E_{\text{CO}_2} + \Delta E_{\text{pop}}, \tag{4}$$

where subscript $T1$ denotes the temporal average over the initial reference period (either 1901–1930 or 1971–2000), and $T2$ over the subsequent reference period (1971–2000 or 2071–2100), E are wildfire emissions, ΔE the change in the temporal average of emissions between the two reference periods, and the subscripts "clim", "CO_2" and "pop" denote the effects of changing climate, CO_2 and human population density.

These latter effects we approximate as:

$$\Delta E_{\text{clim}} = E_{T2}^{cp2} - E_{T1}^{cp2}, \tag{5}$$

$$\Delta E_{\text{CO}_2} = E_{T2}^{p2} - E_{T1}^{p2} - \Delta E_{\text{clim}} = E_{T2}^{p2} - E_{T1}^{p2} - (E_{T2}^{cp2} - E_{T1}^{cp2}), \tag{6}$$

and

$$\Delta E_{\text{pop}} = E_{T2} - E_{T1} - (E_{T2}^{p2} - E_{T1}^{p2}) = E_{T2} - E_{T1} - \Delta E_{\text{clim}} - \Delta E_{\text{CO}_2}. \tag{7}$$

The superscripts $p2$ are for the simulations with population density fixed at year 2000 levels, and $cp2$ for the simulations with both CO_2 and population fixed at 2000 levels. Fire emissions here are computed as the product of burned area and area-specific fuel combustion. Therefore, we can further subdivide the CO_2 effect on emissions between those that work via changing burned area ($\Delta E_{\text{CO}_2}^{\text{b.a.}}$) and those via changing fuel load as the remainder ($\Delta E_{\text{CO}_2}^{\text{f.l.}} = \Delta E_{\text{CO}_2} - \Delta E_{\text{CO}_2}^{\text{a.b.}}$). The former we define as:

$$\Delta E_{\text{CO}_2}^{\text{b.a.}} = \Delta B_{\text{CO}_2}(E_{T1}/B_{T1}), \tag{8}$$

where B_{T1} is the temporal average of burned area during reference period $T1$, and ΔB_{CO_2} the change in burned area due to CO_2 changes, which we approximate in an analogous way to ΔE_{CO_2} as:

$$\Delta B_{\text{CO}_2} = B_{T2}^{p2} - B_{T1}^{p2} - (B_{T2}^{cp2} - B_{T1}^{cp2}). \tag{9}$$

An analogous formulation is used in order discern climate impacts due to burned area from those due to changes in fuel load and its degree of combustion:

$$\Delta E_{\text{clim}}^{\text{b.a.}} = \Delta B_{\text{clim}}(E_{T1}/B_{T1}), \tag{10}$$

with

$$\Delta B_{\text{clim}} = B_{T2}^{cp2} - B_{T1}^{cp2}. \tag{11}$$

We analyse the main driving factors of emissions changes using Eqs. (5–11) for selected large regions, aggregated from the standard GFED regions (Giglio et al., 2010):

1. North America (GFED Boreal and Temperate North America, Central America),
2. South America (GFED Northern and Southern-Hemisphere South America),
3. Europe (same as GFED),
4. Middle East (same as GFED),
5. Africa (GFED Northern and Southern-Hemisphere Africa),
6. North Asia (GFED Boreal and Central Asia),
7. South Asia (GFED South-East and Equatorial Asia),
8. Oceania (GFED Australia and New Zealand).

For a probabilistic analysis of changes in emissions, we follow previous work by Scholze et al. (2006), who counted ensemble members driven by differing climate models where the change of the temporal average between two reference periods was more than one standard deviation of the interannual variability of the first reference period. The authors found a general pattern of increasing wildfire frequency (factional burned area) in arid regions, and a decline at high latitudes and some tropical regions. Here, we apply the method to emissions and use two standard deviations instead in order to ensure that the change is highly significant.

3 Results

3.1 Global emission trends

Global simulated emissions taking into account changes in all factors, climate, CO_2 and population, decline continuously between about 1930 and 2020 for all members of the

ESM ensemble (Fig. 1). Thereafter, emissions approximately stabilize, albeit with a very slight upward trend during 2080–2100 for the moderate greenhouse gas concentrations and climate change scenario RCP4.5 and the central demographic scenario (Fig. 1a). However, different demographic scenarios lead to considerable variations in simulated emissions: while emissions continue to decline until 2100 under high population growth and slow urbanisation (SSP3), the trend of declining emissions is reversed from around 2010 and the total will resume current levels by the end of the 21st century under low population growth and fast urbanisation (SSP5) when taking the ESM ensemble mean. In general, higher population growth drives emissions downward (comparing SSP3 to SSP5), while faster urbanisation contributes to higher wildfire emissions (comparing SSP2 population with fast and slow urbanisation). By the end of the century, different demographic trends generate approximate 0.2 GtC per year difference (ranging from around 1.1 to 1.3 $GtC\,yr^{-1}$) under the moderator climate change RCP4.5. Overall, the range of future emissions spanned by the eight ESMs, but using a single, central population scenario, is less than half of the range spanned by all EMSs and population scenarios combined. None of the simulations has late 21st century emissions reach again the levels present at the beginning of the 20th century (Table 2). Only 9 out of 40 simulations show global average emissions during 2071–2100 higher than during 1971–2000, seven out of which are for low population growth and fast urbanisation, and one for intermediate population growth and fast urbanisation.

Under RCP 8.5, with high greenhouse gas concentrations and climate change, global wildfire emissions start to rise again after 2020 even for the central demographic scenarios (SSP2) and by the end of the 21st century reach levels only slightly below those of the beginning of the 20th century (Fig. 1b). According to this climate change scenario, the world is currently in a temporary minimum of wildfire emissions, independent of demographic scenario or ESM simulation. The population scenario rather determines when emissions are predicted to rise again and how fast emissions increase. For a scenario of high population growth and slow urbanisation (SSP3), emissions rise again after ca. 2070 and reach about 1.2 $GtC\,yr^{-1}$ by the end of the century, while un-

der the fast urbanisation scenarios (SSP5 and SSP2 population with fast urbanisation), they already start rising around 2020. Under RCP8.5, different demographic trends result in different wildfire emissions ranging from 1.2 to 1.5 GtC yr^{-1}. Overall, for 28 out of 40 simulations average emissions during 2071–2100 are higher than during 1971–2000, and for three out of the eight simulations with low population growth and fast urbanisation they are even higher than for 1901–1930 (Table 2).

Simulations with atmospheric CO_2 and population held constant at 2000 levels reveal the impact of climate change on simulated wildfire emissions (Fig. 2a). The climate impact is here shown as the difference in emissions against the average during 1971–2000 (1.28 PgC yr^{-1}, see Table 2). There is a modest positive climate impact on global emissions for RCP8.5, which reaches close to 10 % towards the end of the 21st century for the ESM ensemble mean, with a range between close to 0 and +20 %. For the past, there is no discernable impact of climate change. For RCP4.5, the impact is very small and peaks around 2050 for the ensemble mean, but with a range skewed slightly towards increased emissions.

The CO_2 impact is computed as the difference between two simulations with fixed population density, the one with variable climate and CO_2 minus the one with variable climate but fixed CO_2 (Eq. 6). The resulting emissions differences (Fig. 2b) remain negative throughout the historical period until 2005 because the fixed-CO_2 simulations start out with considerably higher CO_2 levels than the variable-CO_2 ones leading to higher productivity (CO_2 fertilisation, see Hickler et al., 2008; Ahlström et al., 2012), higher fuel load and therefore higher emissions. For RCP8.5, the global CO_2 impact on emissions is about the same as the climate impact, but for RCP4.5 it is much larger. The magnitude of the CO_2 effect itself is climate dependent, which can be seen by the inter-ensemble range, which is caused solely by differences in climate. (All ensemble members use the same atmospheric CO_2 scenarios for a given RCP.) There is also a small interannual variability caused mainly by climate fluctuations, since interannual variations in atmospheric CO_2 are small until 2005 and absent from the scenarios

(Meinshausen et al., 2011). As for climate, there is no discernable CO_2 impact on past emission changes.

Finally, the demographic impact is simulated by the difference between simulations with time varying climate, CO_2 and population, and the corresponding simulations where population is fixed, but the other two vary with time (Eq. 7). As one would expect, the results for the two RCPs are indistinguishable, with a small climate-related ensemble range and a small amount of interannual variability caused by climate fluctuations (Fig. 2c). The simulated demographic impact for the central population scenario is towards declining emissions mainly driven by population growth. After 2050, the effect declines rapidly, and there is a very slight positive trend after ca. 2090 which is due to the leveling off of projected population growth (SSP2) and continuing urbanisation. As can be seen by comparing simulated emissions between the central (SSP2) and the remaining population scenarios (Fig. 1a), the demographic impact varies considerably between scenarios, with a continuing negative impact until 2100 for the scenario with high population growth with slow urbanisation (SSP3), but a positive impact of the demographic change on global emission trends from about 2040 for low population growth with fast urbanisation (SSP5).

Results for the set of sensitivity tests where the parameterisation of SIMFIRE was modified are shown in Fig. 3 for the climate, CO_2 and demographic impacts separately. Note that in this case, simulations are performed with only one ESM (MPI-ESM-LR). The climate impact on emissions is again small for RCP4.5, but discernably positive for RCP8.5 after ca. 2020. The climate impact is hardly affected by changing the SIMFIRE parameterisation. The CO_2 effect is similar to the ensemble mean (Fig. 2b), but with a marked decline after ca. 2080 for RCP8.5. In this case, SIMFIRE optimised against MCD45 burned area shows less of a positive trend after 2020 as a result of CO_2 changes than the standard formulation, and a more pronounced negative effect after 2080. Also, the simulated historical and future demographic impacts are slightly less for MCD45 than for the standard version. The SIMFIRE version with an initial in-

crease in burned area with population density (Eq. 3) has only a very small impact on simulated global emissions.

The recent estimate from the GFED4.0s data set puts the average global wildfire emissions at 1.5 PgC yr^{-1} (released May 2015, 1997–2014 average of savannah, boreal and temperate forest fires combined, against 2.2 PgC yr^{-1} for all biomass burning, van der Werf et al., 2010, updated using Randerson et al., 2012 and Giglio et al., 2013), slightly higher than simulated here (Table 2). During the 20th century, global emissions decrease by around 150 TgC yr^{-1}, a little more than 10 %. The main driving factor of this decrease is growing population, while climate and CO_2 changes have only a very small impact on emissions, as already discussed with Fig. 2. Further analysis of these driving factors (Fig. 4), however, reveals that this small impact is due to compensating action on either burned area (Eqs. 8 and 10) or combustible fuel load (the remainder). Globally, climate had a small positive and CO_2 a slightly smaller negative effect on emissions via burned area. At the same time, climate had a negative and CO_2 a positive impact on combustible fuel load. For the 21st century (Fig. 5), this constellation is predicted to continue, with a somewhat larger demographic impact that is negative across all ensemble members. The overall effect on emissions, however, is small and of uncertain sign (ensemble range including both positive and negative changes). This is because the climate impact and even more both CO_2 effects, acting in opposite directions, increase several fold compared to the situation during the 20th century.

3.2 Driving factors of regional emission changes

By the beginning of the 20th century, the main wildfire emitting region is clearly Africa (Fig. 4), followed by South America, North Asia and Oceania. Emission changes towards the end of the 20th century are mainly due to changes in population density in all regions except for Europe, North America and Oceania where population growth rates are significantly lower. For Europe, climate change has led to an increase in burned area, but an about analogous decrease in fuel load, such that the overall climate effect is small and uncertain. The result for North America is similar, while there is a larger but

still uncertain positive CO_2 effect on fuel load, similar to Oceania and South America. For Oceania the population effect is by far the smallest and the only one uncertain in sign (judging by the ensemble range).

The climate effect via fuel load is negative in all regions, while the climate effect via burned area is almost always positive, except for the Middle East where it is negative but with a large ensemble range spanning both positive and negative, and South Asia, where it is close to zero. We find a negative CO_2 effect via burned area in the tropics (Africa, South America), but a positive effect in the arid sub-tropics and temperate zones (Middle East, North Asia). The positive climate effect can be explained by regional changes in N_{max} (Table 3, cf. Eq. 1), which are always positive, small for changes during the 20th century, but reaching up to over 100 % for Europe from the period 1971–2000 to 2071–2100 under the RCP8.5 climate change scenario. The highest increases are for the northern regions, and the smallest for regions with large deserts, like Africa and Middle East, but starting from a high base. However, climate change can also affect burned area indirectly through vegetation change by changing B or F in Eq. (1), for which a good indicator is the fraction of the total leaf area index that is attributed to grasses ("grass fraction", Table 3). This is because $a(B)$ for grassland and savannahs is about one order of magnitude larger than $a(B)$ for woody biomes (Knorr et al., 2014). There is a general increase in the fraction of woody at the expense of grass vegetation across all except the hyper-arid Middle East region. Here, the grass fraction is by far the highest and the climate too dry to support the expansion of shrubs.

For 1971–2000, simulated wildfire emissions are markedly lower than for the beginning of the 20th century for Africa, South America, South Asia and Middle East (Fig. 5). Of these regions, only Africa is predicted to continue to decline for the entire ensemble range for both RCPs. The main drivers are population growth and CO_2 impact on burned area, partly compensated by increased fuel load. For South America, South Asia and Oceania the pattern is similar, except with a much smaller demographic impact, resulting in an overall change of uncertain direction.

All northern regions (North America, Europe and North Asia) are predicted to increase emissions across the entire ensemble. All of these have a slight positive climate impact, but with large uncertainties, where climate change strongly increases burned area compensated largely by a decrease in fuel load. Since precipitation is predicted to increase in these regions (Table 1), the climate effect is mainly due to increasing temperatures and N_{max} (Tables 1, 3). For North America and North Asia there is a clear positive effect of CO_2 on fuel load which appears to be the main reason for tilting the balance towards emission increases. However, population change plays a rather small role, with a large ensemble range for Europe and North Asia making the sign of the impact uncertain given their slower population growth. For North America, the demographic impact is small, but universally slightly negative. An exception is the region Middle East, which has a large positive CO_2 effect via burned area (cf. Fig. 4).

Overall, there is a marked shift in emissions towards the extra-tropics: while for 1971–2000, the tropics have 700 TgC yr^{-1} emissions vs. 580 for the extra-tropics (ensemble mean), for 2071–2100 the split ranges between 420 tropics vs. 680 extra-tropics for RCP4.5, high population growth/slow urbanisation, and 600 tropics vs. 720 extra-tropics for RCP8.5, low population growth/fast urbanisation. As the regional analysis shows, this change is mainly the result of expanding population in Africa. However, there is also a much stronger negative climate effect on fuel load at high compared to low latitudes (Fig. 6), which to some degree slows down the shift of emissions to the north. This contrasts with a generally positive CO_2 effect across most of the globe, but with about the same magnitude for tropical and extra-tropical vegetated areas. At high latitudes, combustible fuel load is generally much higher than at low latitudes, implying that this is compensated for by a much smaller burned area, leading to overall lower emissions in this region.

3.3 Probabilistic forecast of future emission changes

For simulated emissions during the 20th century, we find that a majority of ensemble members show significant increases (i.e. by more than two standard deviations) for

northern boreal regions and the Tibetan plateau, and decreases for some scattered regions in Europe and China, but in general, changes are small compared to interannual variability (Fig. 7a). For the 21st century, most simulations for both RCP4.5 (Fig. 7b) and RCP8.5 (Fig. 7c) predict a significant decrease in emissions in Africa, mainly north of the equator, and to a lesser degree and mostly for RCP8.5 for North Australian savannahs. The main regions for which a significant increase in fire emissions is predicted are the boreal-forest/tundra transition zones, Europe and China, and arid regions in Central Australia, southern Africa and Central Asia. For the arid regions, however, the increase is much more pronounced for RCP8.5 than for RCP4.5.

These changes in fire emissions during the 21st century relative to current variability can also be analysed by driving factor (Eqs. 5–7). The analysis reveals that increases in emissions in the boreal/tundra transitional zone are mostly due to climate change, except for the more continental and arid north-eastern Siberia. For the rest of the globe, the climate effect has a surprisingly small impact, being confined to narrow bands of arid regions in southern Africa, Australia and the Arabian Peninsula. Climate change also leads to a significant decrease in emissions in northern Africa and the Middle East (Fig. 8a–b, cf. Fig. 5). For RCP4.5, CO_2 has only a small positive impact on emissions, mainly for Central Asia, and a negative impact for African, South American and North Australian tropical savannahs. For RCP8.5, the CO_2 effect has a much bigger impact globally on the relative change of emissions, leading to increased emissions in large regions including Mexico, southern South America, all African, Arabian and Central Asian semi-deserts, most of the southern half of Australia, and north-eastern Siberia. The negative effect is also much more pronounced and comprises most tropical savannahs (Fig. 8c–d). This creates opposing effects for the large zone covering North Africa, Arabia and Central Asia, with climate change leading to a decrease in plant productivity and fuel load (hence lower emissions) against CO_2 change leading to CO_2 fertilisation (hence higher emissions). For the moister and in general much more highly emitting savannahs (van der Werf et al., 2010), the dominant effect comes from CO_2 change and is negative, due to shrub encroachment. This creates an interesting situa-

tion for Australia: in the very north, higher CO_2 leads to shrub encroachment, leading to lower emissions (Fig. 7); in a central zone across the continent, climate change is the leading driver of increased emissions, but for most of the southern half, CO_2 change leads to enhanced water-use efficiency of the already woody vegetation (Morgan et al., 2007) causing the opposite effect compared to the north. The same pattern is repeated for southern Africa, but with a stronger positive climate effect in the central zone. The demographic effect (Fig. 8e) leads to a significant increase in wildfire emissions in Central and Eastern Europe as well as East Asia due to its projected declining population, but a decrease mainly in African savannahs but also Turkey and Afghanistan/southern Central Asia given their projected large increases in population.

4 Discussion

In this study, we find that wildfire emissions declined likely more than 10 % during the course of the 20th century, in agreement with ice core measurements of the isotopic signature of carbon monoxide (Wang et al., 2010). A decline in global wildfire activity since the late 19th century was also suggested by Marlon et al. (2008) based on charcoal records. In the present simulations, the decline is caused overwhelmingly by increasing population density, in agreement with the results of Knorr et al. (2014) who used SIMFIRE alone to simulate burned area, without coupling to LPJ-GUESS, driven by the same historical population data. According to the present study, population effects dominated because a positive effect of climate change on burned area was compensated by a negative effect on fuel load, and a negative effect of CO_2 increase on burned area was compensated a positive effect on fuel load. This broad general pattern, found for the main active wildfire regions, is predicted to continue throughout the 21st century, albeit with much stronger climate and CO_2 effects, while the negative population effect on emissions continues to have about the same magnitude.

This dominant pattern of opposing climate and CO_2 effects, and opposing effects via burned area and fuel load, calls for a mechanistic explanation. A positive impact

of climate change on burned area or numbers of fires is what is commonly expected (Krawchuck et al., 2009; Pechony and Shindell, 2010) and it was found for all regions in agreement with simulated changes in fire risk (N_{max} in Eq. 1). The exception is the Middle East region during the 20th century, with a negative climate impact on burned area, which is likely caused by a decline in fuel continuity which suppresses the spread of fires (reduced F in Eq. 1). A negative climate impact on fuel load is consistent with the widely expected positive climate-carbon cycle feedback (Friedlingstein et al., 2006), whereby rising temperatures increase soil and litter respiration rates, releasing CO_2 from the terrestrial biosphere. The faster decomposition of litter under warmer conditions, incorporated into LPJ-GUESS (Smith et al., 2001), leads to a reduction in fuel available for combustion (Knorr et al., 2012). Since combustion by fire is nothing more than a shortcut for litter decomposition, higher temperatures simply shift the balance between the two processes towards microbial decomposition. However, the opposite climate effect could also be expected, where warming leads to increased productivity in boreal, temperature-limited ecosystems, leading to increased fuel production (Pausas and Ribeiro, 2013). For the present study, at least, this situation does not play a global role and is only found for scattered regions of north-eastern Canada and northern Russia (Fig. 6b).

A positive effect of CO_2 on fuel load, which is found to be active almost everywhere across the globe, is fully consistent with the notion of CO_2 fertilisation of the terrestrial biosphere (Long et al., 1996; Körner 2000), whereby higher atmospheric CO_2 concentrations increase the rate of carboxylation, increasing net primary production and thus fuel load (Hickler et al., 2008). However, we also find a negative impact of rising CO_2 on wildfire emissions for all tropical savannah ecosystems, which outweighs the positive impact through increasing fuel load and is caused by an increase in the dominance of woody at the expense of grass vegetation. This phenomenon of shrub encroachment, or woody thickening, in tropical savannahs has been repeatedly observed in field studies (Wigley et al., 2010; Bond and Midgley, 2012) and frequently attributed to CO_2 enrichment of the atmosphere (Morgan et al., 2007; Buitenwerf et al., 2012). This

link is less observed for arid savannahs (Bond and Midgley, 2012), consistent with the finding here that in the most arid regions, no decrease in the grass fraction is predicted.

On a global scale, according to the present simulations, the level of future wildfire emissions is highly uncertain for a scenario of moderate greenhouse gas increases (RCP4.5), with the ensemble mean showing slightly lower emissions towards the end of the 21st as opposed to the end of the 20th century. For a high, business-as-usual scenario of greenhouse gas forcing (RCP8.5), the ensemble mean points towards an increase across the same time span, but with a range including both positive and negative changes. There is also a general trend towards increases during the second half of this century. The slight bias towards increased emissions is the result of a combination of increased fire risk due to warming, and increased fuel load due to CO_2 fertilisation, but with population growth, woody thickening and faster litter decomposition all counteracting. We therefore find that climatic impacts on fire risk are only one of many, often opposing factors that might lead to increased wildfire emissions in the future.

The future demographic dynamics can lead to a wide range of future wildfire emissions. In addition to its indirect impact on wildfire emissions through interactions with economic and technological changes contributing to GHGs emissions and climate change, changes in population size and spatial distribution play a direct and important role for fire prevalence, as an ignition source but predominantly as fire suppressors. While fertility decline is occurring in almost all global regions, the population momentum will continue to drive global population size upward for at least some years and likely contribute to continuously declining wildfire frequencies. The uncertainty of future population dynamics, however, leads to a wide range of population trends and causes large variations in simulated wildfire emissions. Moreover, the same changes in population sizes can result in rather different emissions due to variations in spatial population distribution, particularly through different urbanisation patterns. While the whole world is expected to be further urbanised, variations in speed and patterns of urbanisation across regions and over time can lead to significantly different wildfire patterns.

Simulated emissions presented here generally agree with similar results with a coupled fire-vegetation-biogeochemical model by Kloster et al. (2012), insofar as climate only starts to impact on fire during the course of the 21st century, but not before, and that changes in population density generally lead to lower emissions. The difference is that in the present study, climate has a much smaller impact on emissions, ranging between 0 and +20 % for RCP8.5 and few percent at most for RCP4.5. A similar study reporting simulations of increasing fire emissions for Europe (Migliavacca et al., 2013a) reports an increase for Europe of about 15 $TgCyr^{-1}$ until the late 21st century, when measured for the same reference period as here, which is within the ensemble range found in this study. Even though they used the same Community Land Model, their fire parameterisation (Migliavacca et al., 2013b) differed from the one used by Kloster et al. (2012).

The difference between the present study and the one by Kloster and co-workers might be due to the pronounced negative effect of temperature change on fuel load, and of CO_2 on burned area, found here. Another important difference is their study included deforestation fires, and employed the more common approach of representing the impact of population density by a combination of number of ignitions times an explicit function of fire suppression, the combination of which leads to a small decrease in emissions during the 21st century. No decline is simulated during the 20th century, neither due to changing population density, nor land use. This study, by contrast, uses a semi-empirical approach with a functional form of the relationship between burned area and population density derived by optimisation against observed burned area and simulates the historical decline that is suggested on the basis of ice core and charcoal records. As discussed by Knorr et al. (2014) and Bistinas et al. (2014), evidence is lacking whether increases in ignitions actually lead to increased fire frequency on a global scale.

An important outcome of this study is that it predicts are large shift in fire emissions from the tropics towards the extra-tropics, driven by two coinciding effects causing a secular decline in emissions in African savannahs and grasslands: CO_2 increases driv-

ing woody thickening, in turn making the vegetation less flammable (Bond and Midgley, 2012), and population growth leading to decreased burned area (Archibald et al., 2008). The impact of this shift on the global budget of carbon emissions from wildfires is so large because these regions currently have by far the largest emissions worldwide (van der Werf et al., 2010). In agreement with observed evidence (Bond and Midgley, 2012), the negative CO_2 effect on emissions via burned area is limited to the semi-humid tropics and does not play a role either in the most arid regions, nor at higher latitudes. It is also not simulated for South Asia, where most of the potential semi-humid grasslands and savannahs have long been converted to agriculture. For the mostly arid region Middle East, we find that a strong positive CO_2 effect via burned area is the larger contributor to emission change during the 20th century, and the biggest during the 21st. This leads to a marked increase in emissions for RCP8.5, outcompeting negative impacts of growing population and climate change on fuel load and driven by a marked decline in precipitation (Table 1), while during the 20th century, there is a marked negative impact of climate change on burned area. Here, CO_2 fertilisation leads to denser vegetation, increasing fuel continuity (higher F in Eq. 1), thus leading to higher burned area, while decreasing precipitation results in a lower F. To a lesser extent this is simulated for North Asia, which also contains large, highly arid regions, but with a positive ensemble-mean climate effect on burned area. For both regions, however, the ensemble spread is very large making the projections highly uncertain.

For Australia, we find an interesting zonal pattern of changing effects from the northern savannahs to the arid southern coast. In the very north, woody thickening due to higher CO_2 leads to decreased emissions through decreased burned area, with negligible climate effects. This is followed by a central zone where both climate and CO_2 change lead to increased emissions, and a third zone comprising the southern half of the Australian interior where CO_2 fertilisation leads to increased emissions via higher productivity. Population change plays almost no role for changing emissions in this region. As a result, the north is predicted to decrease significantly in emissions, while for the central zone where climate and CO_2 effects overlap, and for the south there is no

clear signal in the prediction. A similar tri-zonal pattern is also predicted for southern Africa stretching from the Miombo woodlands across the Kalahari to the Cape region.

5 Conclusions

We find that since the early 20th century, wildfire emissions have been steadily declining due to expanding human population, but that this decline will only continue if climate change and atmospheric CO_2 rise is limited to low or low/moderate levels, population continues to grow and urbanisation follows a slow pathway in the next decades. Otherwise, it is likely that the world is currently in a historic minimum regarding wildfire emissions, and the current declining emission trend will reverse in the future at higher latitudes, departing from the current domination of African savannahs. Emissions, however, are unlikely until 2100 to again reach early 20th century levels. The predictions are based on an ensemble of climate and population/urbanisation projections, but a single fire model albeit tested for the impact of different parameterisations. The results generally show a large ensemble spread, and also reveal widely opposing factors influencing future emissions, complicating the task of predicting future wildfire emissions. We find that apart from climate leading to higher fire risk, equally important factors on a global scale are demographic change, woody thickening in savannahs with higher CO_2 levels, and faster woody or grass litter turnover in a warmer climate, both leading to declining emission, as well as CO_2 fertilisation generally leading to higher fuel loads or fuel continuity and thus increased emissions. Therefore, the common view of climate warming as the dominant driver of higher future wildfire emissions cannot be supported.

Author contributions. W. Knorr conceived the study, carried out model runs, performed the analysis and wrote the first full draft of the manuscript, L. Jiang provided the population scenarios, all authors contributed to discussions of results and writing.

Acknowledgements. This work was supported by EU contracts 265148 (Pan-European Gas-Aerosol-climate interaction Study, PEGASOS) and grant 603542 (Land-use change: assessing

the net climate forcing, and options for climate change mitigation and adaptation, LUC4C). We thank Thomas Hickler for pointing out relevant literature on woody thickening.

References

Ahlström, A., Schurgers, G., Arneth, A., and Smith, B.: Robustness and uncertainty in terrestrial ecosystem carbon response to CMIP5 climate change projections, Environ. Res. Lett., 7, 044008, doi:10.1088/1748-9326/7/4/044008, 2012.

Archibald, S., Roy, D. P., van Wilgen, B. W., and Scholes, R. J.: What limits fire? An examination of drivers of burnt area in Southern Africa, Glob. Change Biol, 15, 613–630, 2008.

Arneth, A., Harrison, S. P., Zaehle, S., Tsigaridis, K., Menon, S., Bartlein, P. J., Feichter, J., Korhola, A., Kulmala, M., O'Donnell, D., Schurgers, G., Sorvari, S., and Vesala, T.: Terrestrial biogeochemical feedbacks in the climate system, Nat. Geosci., 3, 525–532, 2010.

Bistinas, I., Harrison, S. P., Prentice, I. C., and Pereira, J. M. C.: Causal relationships versus emergent patterns in the global controls of fire frequency, Biogeosciences, 11, 5087–5101, doi:10.5194/bg-11-5087-2014, 2014.

Bond, W. J. and Midgley, G. F.: Carbon dioxide and the uneasy interactions of trees and savannah grasses, Philos. T. R. Soc. B, 367, 601–612, 2012.

Bowman, D. M. J. S., Balch, J. K., Artaxo, P., Bond, W. J., Carlson, J. M., Cochrane, M. A., D'Antonio, C. M., DeFries, R. S., Doyle, J. C., Harrison, S. P., Johnston, F. H., Keeley, J. E., Krawchuk, M. A., Kull, C. A., Marston, J. B., Moritz, M. A., Prentice, I. C., Roos, C. I., Scott, A. C., Swetnam, T. W., van der Werf, G. R., and Pyne, S. J.: Fire in the Earth System, Science, 324, 481–484, 2009.

Buitenwerf, R., Bond, W. J., Stevens, N., and Trollope, W. S. W.: Increased tree densities in South African savannas: >50 years of data suggests CO_2 as a driver, Glob. Change Biol., 18, 675–684, 2012.

Friedlingstein, P., Cox, P. M., Betts, R. A., Bopp, L., von Bloh, W., Brovkin, V., Cadule, P., Doney, S., Eby, M., Fung, I., Bala, G., John, J., Jones, C. D., Joos, F., Kato, T., Kawamiya, M., Knorr, W., Lindsay, K., Matthews, H. D., Raddatz, T., Rayner, P. J., Reick, C., Roeckner, E., Schnitzler, K.-G., Schnur, R., Strassmann, K., Weaver, A. J., Yoshikawa, C., and Zeng, N.: Climate–carbon cycle feedback analysis, results from the C4MIP model intercomparison, J. Climate, 19, 3337–3353, 2006.

Giglio, L., Randerson, J. T., van der Werf, G. R., Kasibhatla, P. S., Collatz, G. J., Morton, D. C., and DeFries, R. S.: Assessing variability and long-term trends in burned area by merging multiple satellite fire products, Biogeosciences, 7, 1171–1186, doi:10.5194/bg-7-1171-2010, 2010.

Giglio, L., Randerson, J. T., and van der Werf, G. R.: Analysis of daily, monthly, and annual burned area using the fourth-generation global fire emissions database (GFED4), J. Geophys. Res.-Biogeo., 118, 317–328, 2013.

Harris, I., Jones, P. D., Osborn, T. J., and Lister, D. H.: Updated high-resolution grids of monthly climatic observations – the CRU TS3.10 Dataset, Int. J. Climatol., 34, 623–642, 2014.

Hickler, T., Smith, B., Prentice, I. C., Mjöfors, K., Miller, P., Arneth, A., and Sykes, M. T.: CO_2 fertilization in temperate FACE experiments not representative of boreal and tropical forests, Glob. Change Biol., 14, 1531–1542, 2008.

Hurtt, G. C., Chini, L. P., Frolking, S., Betts, R. A., Feddema, J., Fischer, G., Fisk, J. P., Hibbard, K., Houghton, R. A., Janetos, A., Jones, C. D., Kindermann, G., Kinoshita, T., Goldewijk, K. K., Riahi, K., Shevliakova, E., Smith, S., Stehfest, E., Thomson, A., Thornton, P., van Vuuren, D. P., and Wang, Y. P.: Harmonization of land-use scenarios for the period 1500–2100: 600 years of global gridded annual land-use transitions, wood harvest, and resulting secondary lands, Climatic Change, 109, 117–161, 2011.

Jiang, L.: Internal consistency of demographic assumptions in the shared socioeconomic pathways, Popul. Environ., 35, 261–285, 2014.

Kasischke, E. S. and Penner, J. E.: Improving global estimates of atmospheric emissions from biomass burning, J. Geophys. Res., 109, D14S01, doi:10.1029/2004JD004972, 2004.

Klein Goldewijk, K., Beusen, A., and Janssen, P.: Long-term dynamic modeling of global population and built-up area in a spatially explicit way: HYDE 3.1, Holocene, 20, 565–573, 2010.

Kloster, S., Mahowald, N. M., Randerson, J. T., and Lawrence, P. J.: The impacts of climate, land use, and demography on fires during the 21st century simulated by CLM-CN, Biogeosciences, 9, 509–525, 2012, http://www.biogeosciences.net/9/509/2012/.

Knorr, W., Lehsten, V., and Arneth, A.: Determinants and predictability of global wildfire emissions, Atmos. Chem. Phys., 12, 6845–6861, doi:10.5194/acp-12-6845-2012, 2012.

Knorr, W., Kaminski, T., Arneth, A., and Weber, U.: Impact of human population density on fire frequency at the global scale, Biogeosciences, 11, 1085–1102, doi:10.5194/bg-11-1085-2014, 2014.

Knorr, W., Jiang, L., and Arneth, A.: Demographic controls of future fire risk, in review, 2015.
Körner, C.: Biosphere responses to CO_2 enrichment, Ecol. Appl., 10, 1590–1619, 2000.
Krawchuk, M. A., Moritz, M. A., Parisien, M. A., Van Dorn, J., and Hayhoe, K.: Global Pyrogeography: the Current and Future Distribution of Wildfire, Plos One, 4, e5102, doi:10.1371/journal.pone.0005102, 2009.
Langmann, B., Duncan, B., Textor, C., Trentmann, J., and van der Werf, G. R.: Vegetation fire emissions and their impact on air pollution and climate, Atmos. Environ., 43, 107–116, 2009.
Long, S. P., Osborne, C. P., and Humphries, S. W.: Photosynthesis, rising atmospheric carbon dioxide concentration and climate change, in: Global change: Effects on coniferous forests and grasslands, edited by: Breymeyer, A. I., Hall, D. O., Melillo, J. M., and Âgren, G. I., Scope, Wiley & Sons, New York, 1996.
Marlon, J. R., Bartlein, P. J., Carcaillet, C., Gavin, D. G., Harrison, S. P., Higuera, P. E., Joos, F., Power, M. J., and Prentice, I. C.: Climate and human influences on global biomass burning over the past two millennia, Nat. Geosci., 1, 697–702, 2008.
Meinshausen, M., Smith, S. J., Calvin, K., Daniel, J. S., Kainuma, M. L. T., Lamarque, J.-F., Matsumoto, K., Montzka, S. A., Raper, S. C. B., Riahi, K., Thomson, A., Velders, G. J. M., and van Vuuren, D. P. P.: The RCP greenhouse gas concentrations and their extensions from 1765 to 2300, Climatic Change, 109, 213–241, 2011.
Migliavacca, M., Dosio, A., Camia, A., Hobourg, R., Houston Durtant, T., Kaiser, J. W., Khabarov, N., Krasovskii, A. A., Marcolla, B., Miguel-Ayanz, J., Ward, D. S., and Cescatti, A.: Modeling biomass burning and related carbon emissions during the 21st century in Europe, J. Geophys. Res., 118, 1732–1747, 2013a.
Migliavacca, M., Dosio, A., Kloster, S., Ward, D. S., Camia, A., Houborg, R., Houston Durtant, T., Khabarov, N., Krasovskii, A. A., San Miguel-Ayanz, J., and Cescatti, A.: Modeling burned area in Europe with the Community Land Model, J. Geophys. Res., 118, 265–279, 2013b.
Morgan, J. A., Milchunas, D. G., LeCain, D. R., West, M., and Mosier, A. R.: Carbon dioxide enrichment alters plant community structure and accelerates shrub growth in the shortgrass steppe, P. Natl. Acad. Sci. USA, 104, 14724–14729, 2007.
Moritz, M. A., Parisien, M.-A., Batllori, E., Krawchuk, M. A., Van Dorn, J., Ganz, D. J., and Hayhoe, K.: Climate change and disruptions to global fire activity, Ecosphere, 3, 49, doi:10.1890/ES11-00345.1, 2012.
O'Neill, B., Carter, T. R., Ebi, K. L., Edmonds, J., Hallegatte, S., Kemp-Bendedict, E., Kriegler, E., Mearns, L., Moss, R., Riahi, K., van Ruijven, B., and van Vuuren, D.: Meeting Report of

the Workshop on The Nature and Use of New Socioeconomic Pathways for Climate Change Research, Boulder, CO, November 2–4 2011, available at: https://www2.cgd.ucar.edu/sites/default/files/iconics/Boulder-Workshop-Report.pdf (last access: 9 September 2015, National Center for Atmospheric Research (NCAR), Boulder, USA, 2012.
Pausas, J. G. and Ribeiro, E.: The global fire–productivity relationship, Global Ecol. Biogeogr., 22, 728–736, 2013.
Pechony, O. and Shindell, D. T.: Driving forces of global wildfires over the past millennium and the forthcoming century, P. Natl. Acad. Sci. USA, 107, 19167–19170, 2010.
Ramankutty, N. and Foley, J. A.: Estimating historical changes in global land cover: Croplands from 1700 to 1992, Global Biogeochem. Cy., 13, 997–1027, 1999.
Randerson, J., Chen, Y., van der Werf, G. R., Rogers, B. M., and Morton, D. C.: Global burned area and biomass burning emissions from small fires, J. Geophys. Res., 117, G04012, doi:10.1029/2012JG002128, 2012.
Roy, D. P., Boschetti, L., Justice, C. O., and Ju, J.: The collection 5 MODIS burned area product – Global evaluation by comparison with the MODIS active fire product, Remote Sens. Environ., 112, 3690–3707, 2008.
Scholze, M., Knorr, W., Arnell, N. W., and Prentice, I. C.: A climate-change risk analysis for world ecosystems, P. Natl. Acad. Sci. USA, 103, 13116–13120, 2006.
Smith, B., Prentice, C., and Sykes, M.: Representation of vegetation dynamics in modelling of terrestrial ecosystems: comparing two contrasting approaches within European climate space, Global Ecol. Biogeogr., 10, 621–637, 2001.
Taylor, K. E., Stouffer, R. J., and Meehl, G. A.: An overview of CMIP5 and the experiment design, B. Am. Meteorol. Soc., 93, 485–498, 2012.
Thonicke, K., Spessa, A., Prentice, I. C., Harrison, S. P., Dong, L., and Carmona-Moreno, C.: The influence of vegetation, fire spread and fire behaviour on biomass burning and trace gas emissions: results from a process-based model, Biogeosciences, 7, 1991–2011, doi:10.5194/bg-7-1991-2010, 2010.
van der Werf, G. R., Randerson, J. T., Giglio, L., Collatz, G. J., Mu, M., Kasibhatla, P. S., Morton, D. C., DeFries, R. S., Jin, Y., and van Leeuwen, T. T.: Global fire emissions and the contribution of deforestation, savanna, forest, agricultural, and peat fires (1997–2009), Atmos. Chem. Phys., 10, 11707–11735, doi:10.5194/acp-10-11707-2010, 2010.
van Vuuren, A. J., Edmonds, J., Kainuma, M., Riahi, K., Thomson, A., Hibbard, K., Hurtt, G. C., Kram, T., Krey, V., Lamarque, J. F., Masui, T., Meinshausen, M., Naicenovic, N., Smith, S. J.,

and Rose, S. K.: The representative concentration pathways: an overview, Climatic Change, 109, 5–31, 2011.

Wang, Z., Chappellaz, J., Park, K., and Mak, J. E.: Large variations in Southern Hemisphere biomass burning during the last 650 years, Science, 330, 1663–1666, 2010.

Wigley, B. J., Bond, W. J., and Hoffman, M. T.: Thicket expansion in a South African savanna under divergent land use: local vs. global drivers?, Glob. Change Biol., 16, 964–976, 2010.

Table 1. Simulated changes in climate by region.

Region	historical[2]		RCP4.5[3]		RCP8.5[3]	
	Absolute change in annual-mean temperature [K][1]					
North America	0.62	(0.03, 1.18)	3.15	(1.88, 4.90)	5.70	(3.78, 7.97)
Europe	0.50	(−0.20, 1.00)	2.56	(1.77, 3.83)	4.53	(3.46, 6.26)
North Asia	0.51	(0.07, 0.98)	3.25	(2.13, 4.81)	5.69	(3.91, 7.63)
Middle East	0.50	(0.09, 0.86)	2.71	(1.82, 3.78)	5.05	(3.68, 6.33)
South America	0.43	(0.07, 0.78)	2.36	(1.65, 3.19)	4.34	(2.83, 5.39)
Africa	0.47	(0.08, 0.72)	2.54	(1.77, 3.34)	4.67	(3.48, 5.87)
South Asia	0.37	(0.01, 0.65)	2.28	(1.60, 3.06)	4.07	(2.95, 5.09)
Oceania	0.44	(0.17, 0.74)	2.18	(1.35, 2.83)	4.16	(2.83, 5.35)
Globe	0.50	(0.08, 0.83)	2.77	(1.83, 3.89)	5.01	(3.49, 6.48)
	Relative change in mean annual precipitation[3]					
North America	−0.5 %	(−1.8 %, 1.6 %)	4.6 %	(−2.1 %, 7.6 %)	5.3 %	(−5.7 %, 10.8 %)
Europe	−1.0 %	(−4.5 %, 1.5 %)	1.9 %	(−3.0 %, 10.7 %)	0.6 %	(−5.6 %, 13.1 %)
North Asia	−0.8 %	(−3.3 %, 1.0 %)	9.4 %	(5.8 %, 15.1 %)	13.8 %	(8.2 %, 19.7 %)
Middle East	−6.4 %	(−11.8 %, 0.9 %)	−6.0 %	(−17.0 %, 5.7 %)	−10.7 %	(−28.3 %, 0.0 %)
South America	−2.5 %	(−6.8 %, −0.9 %)	−0.7 %	(−8.8 %, 11.7 %)	−1.3 %	(−10.6 %, 14.3 %)
Africa	−2.7 %	(−9.3 %, 0.1 %)	1.4 %	(−6.3 %, 5.0 %)	2.7 %	(−5.0 %, 9.6 %)
South Asia	−1.2 %	(−6.0 %, 1.8 %)	8.3 %	(4.9 %, 12.8 %)	14.5 %	(9.0 %, 22.3 %)
Oceania	−1.5 %	(−7.2 %, 2.7 %)	−1.9 %	(−27.2 %, 6.6 %)	−6.7 %	(−38.3 %, 11.8 %)
Globe	−1.8 %	(−3.2 %, 0.1 %)	3.3 %	(−1.1 %, 5.6 %)	4.7 %	(0.8 %, 7.6 %)

[1] Mean across 8-ESM ensemble, ensemble minimum and maximum in parentheses.
[2] Changes from 1901–1930 to 1971–2000.
[3] Changes from 1971–2000 to 2071–2100.

Table 2. Temporal average of global wildfire emissions in TgC yr^{-1} by time period, scenario and ESM[9].

Period	RCP	Population growth	Urban-ization	ESM Ensemble	MPI-ESM-LR[1]	CCSM4[2]	CSIRO-Mk3.6[3]	EC-EARTH[4]	CNRM-CM5[5]	GISS-E2-R[6]	IPSL-CM5A-MR[7]	HADGEM2-ES[8]
1901–1930	–	Historical	Historical	**1.43**	**1.44**	**1.42**	**1.46**	**1.42**	**1.43**	**1.42**	**1.44**	**1.39**
1971–2000				*1.28*	*1.32*	*1.27*	*1.28*	*1.29*	*1.29*	*1.25*	*1.28*	*1.27*
2071–2100	4.5	low	fast	**1.31**	**1.36**	**1.31**	1.27	**1.31**	**1.29**	**1.27**	**1.33**	**1.36**
		intermediate	fast	1.27	1.32	1.27	1.23	1.26	1.26	1.23	**1.29**	**1.32**
		intermediate	central	1.22	1.26	1.22	1.17	1.20	1.20	1.18	1.23	1.27
		intermediate	slow	1.17	1.21	1.16	1.13	1.15	1.15	1.13	1.18	1.21
		high	slow	1.11	1.15	1.11	1.07	1.09	1.09	1.07	1.12	1.16
	8.5	low	fast	**1.43**	**1.52**	**1.45**	**1.41**	**1.38**	**1.41**	**1.37**	**1.42**	**1.50**
		intermediate	fast	**1.39**	**1.47**	**1.41**	**1.38**	**1.34**	**1.36**	**1.33**	**1.38**	**1.46**
		intermediate	central	**1.33**	**1.41**	**1.36**	**1.32**	**1.29**	**1.30**	**1.28**	**1.33**	**1.40**
		intermediate	slow	**1.28**	1.35	**1.31**	1.26	1.24	**1.25**	1.23	1.27	**1.35**
		high	slow	1.22	1.29	1.24	1.19	1.18	1.19	1.18	1.22	**1.28**

[1] Max Planck Institute for Meteorology;
[2] National Centre for Atmospheric Research;
[3] Commonwealth Scientific and Industrial Research Organization in collaboration with Queensland CSIRO Climate Change Centre of Excellence;
[4] EC-EARTH consortium;
[5] Centre National de Recherches Météorologiques/Centre Européen de Recherche et Formation Avancée en Calcul Scientifique;
[6] NASA Goddard Institute for Space Studies;
[7] Institut Pierre-Simon Laplace;
[8] Met Office Hadley Centre;
[9] Emissions larger than during 1971–2000 (italics) are shown in bold.

Table 3. Changes in climatic and vegetation fire risk[1].

Region	1901–1930		1971–2000		RCP4.5 [2]		RCP8.5 [2]	
	Mean annual-maximum Nesterov index							
North America	153	(143, 165)	160	(148, 170)	204	(178, 236)	250	(211, 327)
Europe	80	(73, 93)	83	(77, 87)	120	(94, 152)	166	(103, 228)
North Asia	146	(142, 154)	149	(144, 155)	188	(163, 220)	227	(185, 292)
Middle East	2878	(2731, 3184)	2923	(2831, 3169)	3201	(2962, 3443)	3401	(3060, 3776)
South America	240	(223, 254)	248	(233, 272)	298	(258, 338)	348	(265, 432)
Africa	1461	(1379, 1491)	1481	(1434, 1530)	1618	(1519, 1728)	1719	(1566, 1898)
South Asia	288	(272, 314)	296	(276, 318)	332	(300, 368)	368	(312, 449)
Oceania	570	(509, 605)	586	(535, 625)	671	(553, 851)	795	(598, 1085)
Globe	726	(700, 765)	740	(715, 773)	827	(767, 878)	903	(817, 1007)
	Grass fraction							
North America	30 %	(28 %, 31 %)	28 %	(27 %, 29 %)	22 %	(20 %, 23 %)	20 %	(19 %, 22 %)
Europe	14 %	(13 %, 15 %)	12 %	(11 %, 13 %)	10 %	(9 %, 12 %)	11 %	(9 %, 12 %)
North Asia	36 %	(34 %, 37 %)	33 %	(33 %, 34 %)	21 %	(17 %, 23 %)	16 %	(13 %, 18 %)
Middle East	75 %	(74 %, 76 %)	76 %	(75 %, 77 %)	77 %	(76 %, 79 %)	76 %	(75 %, 78 %)
South America	26 %	(25 %, 28 %)	23 %	(23 %, 24 %)	16 %	(15 %, 16 %)	13 %	(12 %, 14 %)
Africa	57 %	(56 %, 59 %)	53 %	(53 %, 54 %)	40 %	(39 %, 42 %)	34 %	(32 %, 36 %)
South Asia	26 %	(25 %, 27 %)	23 %	(23 %, 24 %)	17 %	(16 %, 18 %)	15 %	(14 %, 15 %)
Oceania	82 %	(79 %, 85 %)	81 %	(79 %, 83 %)	76 %	(74 %, 81 %)	69 %	(65 %, 76 %)
Globe	43 %	(43 %, 44 %)	41 %	(41 %, 41 %)	33 %	(32 %, 34 %)	29 %	(28 %, 31 %)

[1] Mean across 8-ESM ensemble, ensemble minimum and maximum in parentheses.
[2] Temporal average for 2071–2100.

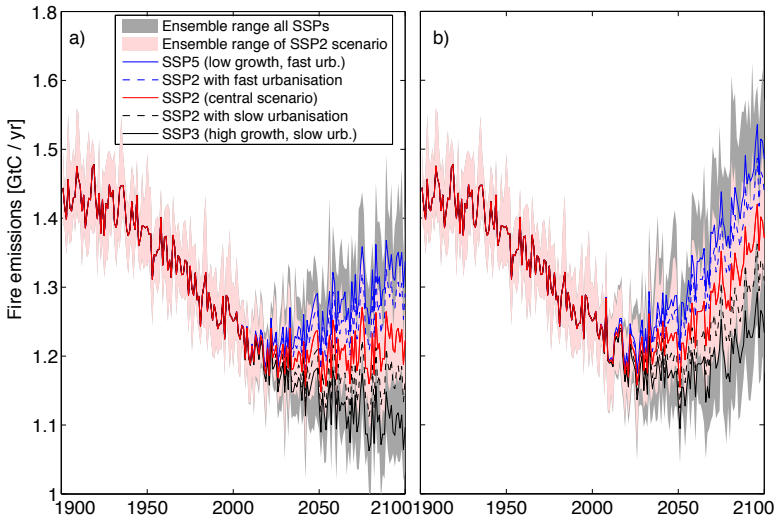

Figure 1. Simulated global wildfire emissions 1900 to 2100. Shaded areas are for the range of ensemble members either across all ESMs using only the central population scenario SSP2, or across ESMs and all population scenarios. Lines show ensemble averages for specific population scenarios. **(a)** RCP4.5 greenhouse gas concentrations and climate change; **(b)** RCP8.5.

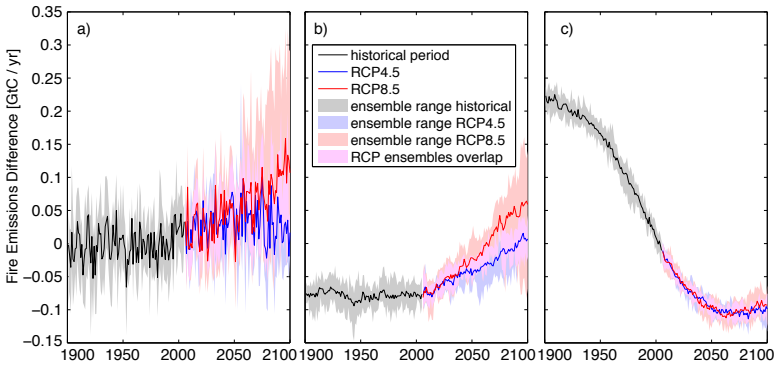

Figure 2. Effects of different factors on global emissions for historical change (until 2005) and two future climate change scenarios (RCP4.5 and RCP8.5). **(a)** Effect of climate change, **(b)** effect of changing atmospheric CO_2, **(c)** effect of changing human population density. All simulations are for the central SSP2 population scenario. Solid lines for ESM ensemble means and shaded areas for the range across eight ESM simulations each.

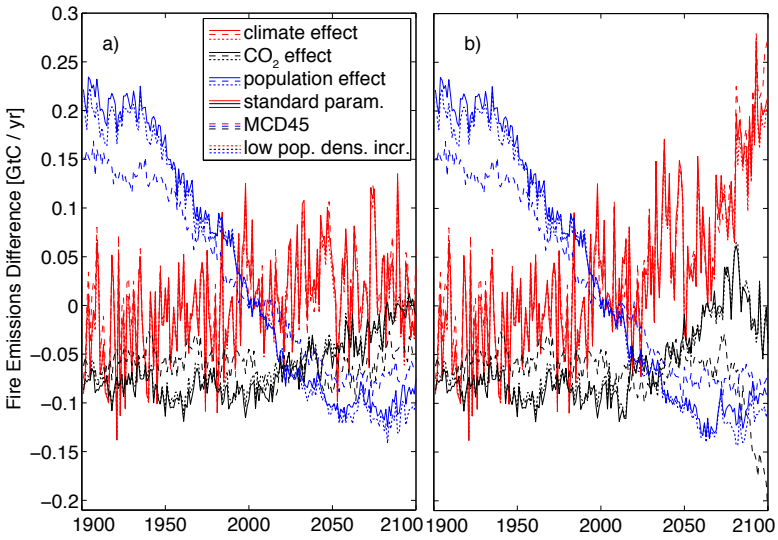

Figure 3. Impact of changing fire model parameterisation on the simulated climate, CO_2 and population effects on emissions. Standard parameterisation of SIMFIRE optimised against GFED3 burned area, optimisation against MCD45 burned area, and simulation assuming an increasing effect of population density on burned area between 0 and 0.1 inhabitants km^{-2}. **(a)** RCP4.5. **(b)** RCP8.5.

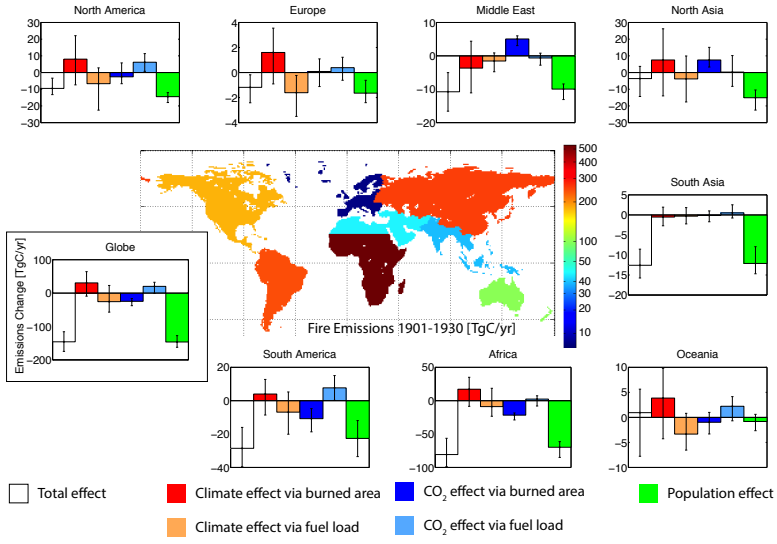

Figure 4. Regional wildfire emissions during 1901–1930 for eight regions and global and regional changes, average 1971–2000 minus average 1901–1930, for ensemble mean (white/coloured bars) and range across ensemble comprising eight ESMs (error bars), in TgC yr^{-1}. The change in emissions is further subdivided into climate effect due to changes in burned area or changes in combusted fuel per burned area, effect of atmospheric CO_2 change due to changed burned are or fuel combustion, and population effect.

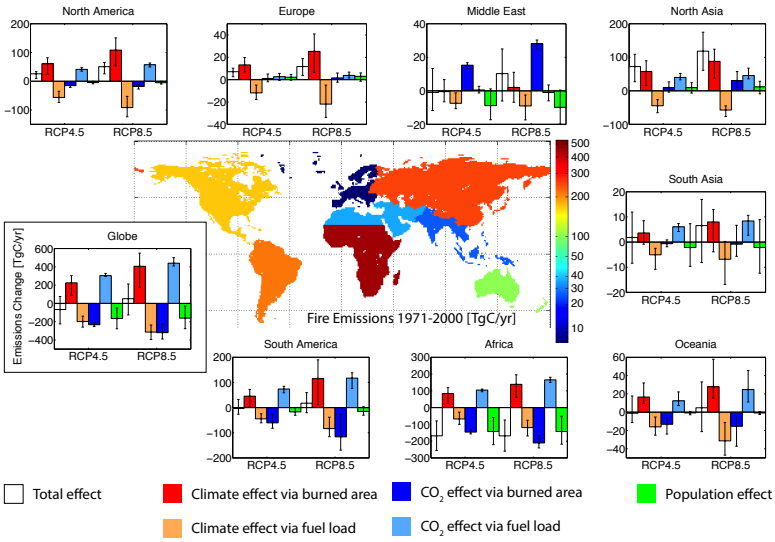

Figure 5. As previous figure, but for average emissions during 1971–2000 and changes as 2071–2100 minus 1971–2000 averages, both differentiated between RCP4.5 and RCP8.5 climate scenarios. In this case, the ensemble is across eight ESMs times five population scenarios.

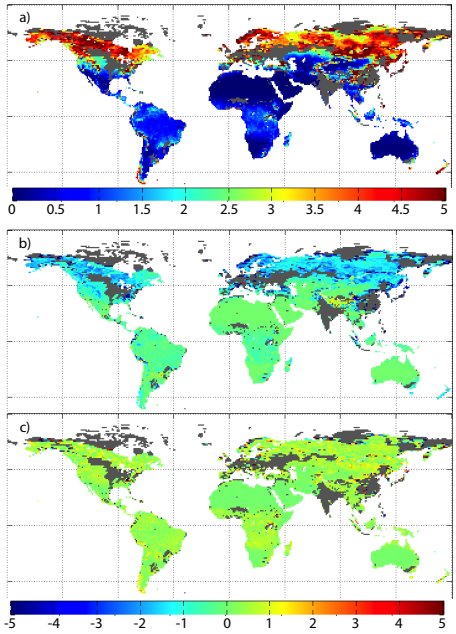

Figure 6. Ensemble-mean combustible fuel load in kgC m^{-2} and change due to climate and CO_2 effects. **(a)** Average emissions 1971–2000; **(b)** change from 1971–2000 to 2071–2100 for RCP8.5 due to climate effect; **(c)** same as **(b)** but due to CO_2 effect. Grey areas have no fire or are excluded as dominated by agriculture. Combustible fuel load is the amount of carbon potentially emitted if a fire occurs.

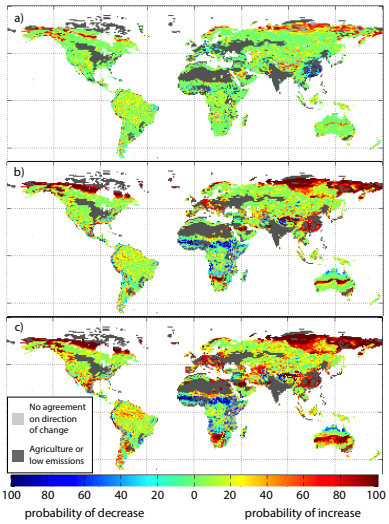

Figure 7. Fraction of ensemble members with either a significant decrease or increase in wildfire emissions (positive or negative change by more than two standard deviations of the interannual variability of the initial period). Agricultural areas and areas with ensemble median emissions less than 10 % of global median during 2071–2100 were excluded. **(a)** Changes from 1901–1930 to 1971–2000; **(b)** changes from 1971–2000 to 2071–2100 for RCP4.5; **(c)** as **(b)** but for RCP8.5.

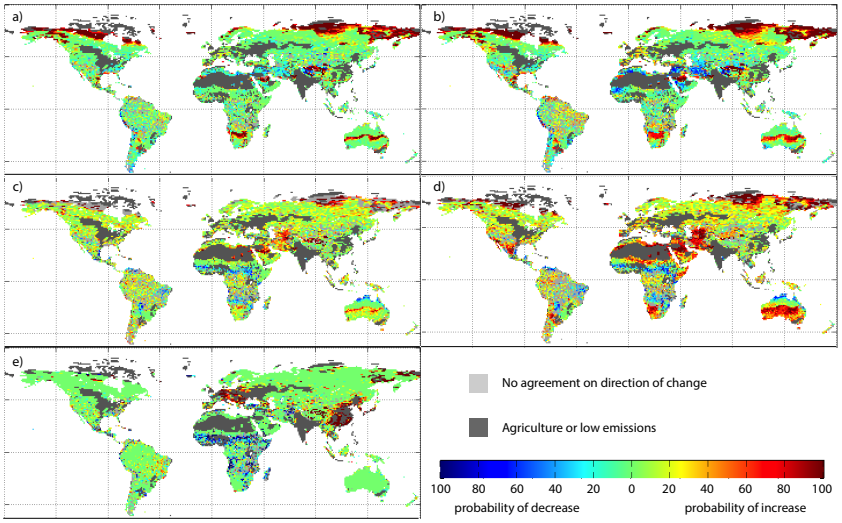

Figure 8. As previous figure, but for emissions changes due to single driving factors. **(a, b)** climate effect, **(c, d)** CO_2 effect, **(e)** population effect; **(a, c)** RCP4.5, **(b, d)** RCP8.